Sensitivity of static stress calculations to the earthquake slip distribution

Sandy Steacy

Geophysics Research Group, University of Ulster, Coleraine, Northern Ireland

David Marsan

Laboratoire de Géophysique Interne et de Tectonophysique, Université de Savoie, France

Suleyman S. Nalbant and John McCloskey

Geophysics Research Group, University of Ulster, Coleraine, Northern Ireland

[1]   The apparent strong correlation between Coulomb stress changes and the spatial distribution of aftershocks suggests the possibility of making near-real-time estimations of areas at risk of experiencing off-fault aftershocks. In order to do this in practice a number of issues must first be addressed, including the extent to which the main shock slip must be known in detail before a meaningful stress map can be constructed. Here we investigate this issue by constructing a time-ordered sequence of slip solutions for the Landers earthquake, computing Coulomb stress changes for each solution, and quantitatively comparing the stress field with the observed aftershocks by (1) resolving the Coulomb stress change onto the aftershock nodal planes and calculating the percentage of events consistent with triggering and (2) constructing a two-dimensional map of Coulomb stress and computing the correlation coefficient between the positive and negative areas and the locations of the aftershocks. We find that slip solutions based on empirical relations and either focal mechanism or moment tensor data produce stress fields inconsistent with the observed spatial distribution of aftershocks, whereas slip solutions incorporating the correct rupture geometry but greatly simplified slip produce stress fields consistent with the aftershock distribution when very near-fault events are excluded. We further find that resolving stress perturbations onto earthquake nodal planes and computing the percentage of events experiencing positive Coulomb stress provides a poor measure of success because of the limited range of structures on which events occur and the compatibility of the main shock stress field with these structures. Our results support the hypothesis that Coulomb stress changes affect the spatial distribution of aftershocks and suggest that meaningful calculations of Coulomb stress can be made as soon as an earthquake's rupture geometry is well constrained.   *INDEX TERMS:* 7209 Seismology: Earthquake dynamics and mechanics; 7215 Seismology: Earthquake parameters; 7223 Seismology: Seismic hazard assessment and prediction; *KEYWORDS:* Coulomb stress, earthquake hazard, aftershocks

Citation: Steacy, S., D. Marsan, S. S. Nalbant, and J. McCloskey (2004), Sensitivity of static stress calculations to the earthquake slip distribution, *J. Geophys. Res.*, *109*, B04303, doi:10.1029/2002JB002365.

1.   Introduction

1.1.   Modeling Static Coulomb Stress

[2]   A relationship between static stress changes and the spatial distribution of aftershocks was first proposed by *Das and Scholz* [1981] following the strike-slip 1968 Borrego Mountain and 1979 Homestead Valley, California, earthquakes. The authors observed that off-fault aftershocks of these events occurred in distinct lobes on both sides of each main shock fault plane with clear gaps between the fault

planes and the lobes and pointed out that the lobes were located in regions where the shear stress had been increased due to slip in the main shocks [*Chinnery*, 1963]. *Stein and Lisowski* [1983] calculated the static Coulomb stress changes for the Homestead Valley event and found that most aftershocks occurred in areas where the stress had increased by 3 bars, and they were nearly absent in regions that experienced stress decreases of 3–5 bars.

[3]   After the 1992 Landers earthquake (M_w = 7.3), *Stein et al.* [1992] demonstrated that smaller events over the preceding 17 years had increased stress at the Landers epicenter and along much of its rupture length. They also showed that the majority of aftershocks occurred in regions

where the stress had increased, including, in particular, the $M_w = 6.4$ Big Bear aftershock that occurred about 3 1/2 hours after the Landers event, 40 km from the fault plane. These observations were supported by *Harris and Simpson* [1992], who found that 4 out of 5 $M > 4.5$ aftershocks had experienced positive Coulomb stress changes ($\Delta CFF = \tau + \mu'\sigma_n$, where τ is the shear stress change in the rake direction of the aftershock, μ' is the effective coefficient of friction, and σ_n is the normal stress change). *King et al.* [1994] used the detailed slip inversion of *Wald and Heaton* [1994] to model the Landers event and observed that aftershocks were abundant where the Coulomb stress on optimally oriented planes increased by more than 0.5 bars and were sparse where it decreased by a similar amount.

[4] Following the Landers event, a number of authors examined the relation between static stress changes and triggering of both aftershocks and main shocks in a variety of tectonic settings. In all cases, they found good qualitative agreement between areas of Coulomb stress increase and triggered earthquakes and, additionally, observed that earthquakes were less likely to occur in stress shadows or areas of Coulomb stress decrease (for recent reviews see *Harris* [1998], *Stein* [1999], and *King and Cocco* [2001]).

[5] Quantifying this relation is more difficult and has been discussed by many authors [e.g., *Reasenberg and Simpson*, 1992; *Harris et al.*, 1995; *Hardebeck et al.*, 1998; *Anderson and Johnson*, 1999; *Seeber and Armbruster*, 2000]. Two main approaches are generally considered: (1) mapping changes in seismicity rates concurrent with the occurrence of the main shock and correlating them with changes in Coulomb stress and (2) computing the Coulomb stress change at the locations of the aftershocks, either by considering optimally oriented planes or by using the focal mechanisms of the aftershocks. Quite generally, the first approach typically shows better success for well constrained (i.e., computed using reliable information on the main shock) Coulomb stress maps than the second. In particular, computation of stress changes on the nodal planes of the aftershocks can exhibit poor success rates. This is partly due to the generally large uncertainties on the focal mechanisms, the ambiguity about which of the two nodal planes is the fault plane, and the fact that such stresses are very poorly estimated for all the aftershocks occurring close to or on the main fault. On the other hand, correlation between seismicity and stress changes can be very good; visual inspection of stress change maps and aftershock epicenter distributions generally show good agreement between the two. However, estimating reliable seismicity rate changes can sometimes prove to be difficult, especially at intermediate to long timescales (weeks to years); see *Marsan* [2003].

[6] The relation between static stress changes and earthquake triggering has important implications for earthquake hazard analysis. *Stein et al.* [1997] and *Nalbant et al.* [1998] examined the interaction of large earthquakes along the North Anatolian Fault Zone in Turkey and demonstrated a strong link between increases in Coulomb stress due to previous earthquakes and the occurrence of later events. Both papers identified the future rupture zone of the 1999 $M = 7.4$ Izmit earthquake as the most likely location for a large event. Following this event, *Hubert-Ferrari et al.* [2000] and *Parsons et al.* [2000] argued that

the earthquake risk in the Marmara Sea, south of Istanbul, had increased as a consequence of Coulomb loading from the Izmit earthquake.

1.2. Coulomb Modeling as a Predictive Tool

[7] Although the relation between Coulomb stress change and main shock–main shock earthquake triggering is difficult to quantify due to insufficient knowledge of the magnitude of Coulomb perturbations with respect to the fault failure stress, the relation between Coulomb stress changes and aftershocks is much simpler as aftershocks are most likely events triggered by the earlier earthquakes in the sequence. Whereas on-fault aftershocks may be caused by stress concentrations on unbroken segments of the main shock rupture plane, the correlation between regions of positive change in Coulomb stress and the locations of off-fault aftershocks supports a relation between them, and suggests that calculation of Coulomb stress changes following large events may constrain the likely locations of off-fault aftershocks. Such a possibility has important consequences for earthquake hazard estimation as convolution of regions of likely aftershocks with site effect data could, for instance, be used to inform emergency services of areas likely to experience future strong shaking (or, perhaps more importantly, regions unlikely to suffer further damage).

[8] In order to assess the scientific feasibility of using the Coulomb stress technique to make probabilistic estimations of aftershock hazard, a number of questions need to be addressed systematically, including the following: How sensitive is the spatial distribution of off-fault aftershocks to the details of the slip distribution? What is the minimum accuracy of the slip distribution that is required to make significant, useful estimations of the forthcoming spatial aftershock distribution? By what extent do these estimations improve as more detailed and reliable slip inversions become available?

[9] These questions are addressed in this paper. Ideally, following a large earthquake, the most accurate slip distribution available should be used to calculate the stress perturbation. At a practical level, however, it is clear that the most accurate possible estimation of the slip distribution will evolve through time as better data become available and more rigorous calculations are undertaken. Such an evolution might take the form: (1) short term (<1 hour), approximate location, magnitude, and focal mechanism; (2) intermediate term (hours to days), improved location, correct nodal plane, and fault geometry; and (3) longer term (hours to weeks), detailed slip models.

[10] To date, stress modeling papers have generally been based on detailed slip distributions calculated months to years following the large earthquake. If, however, the technique is to be used in near real-time to estimate aftershock hazard then either the Coulomb stress calculations must be relatively insensitive to the details of the slip distribution or it must be possible to compute detailed slip distributions quickly and accurately. The latter is becoming increasingly likely, at least for well-recorded teleseismic events, as M. Kikuchi and Y. Yagi have demonstrated by quickly publishing online slip inversions for significant earthquakes (http://www.eic.eri.u-tokyo.ac.jp/EIC/).

[11] In the following, we describe a suite of slip inversions for the Landers ($M_w = 7.3$) earthquake, ranging from a

very quick solution based on the National Earthquake Information Center's focal mechanism to the detailed inversions of *Wald and Heaton* [1994] and *Hernandez et al.* [1999]. For each solution, we compare the stress field caused by the earthquake slip with the observed distribution of aftershocks. We then examine the sensitivity of the results to the coefficient of friction and to the exclusion of on-fault events. Finally, we investigate whether adding the stress perturbation due to the Big Bear (M_w = 6.4) aftershock affects the results.

2. Methodology

[12] Our aim is to assess the extent to which the slip distribution must be known in detail before useful calculations of the stress perturbation can be made. We therefore construct in section 2.1 a time-ordered sequence of slip distributions designed to reflect the successively more detailed information that would have become available following the Landers earthquake. For each slip distribution, we quantitatively compare the resulting stress field with the observed distribution of aftershocks by (1) resolving the Coulomb stress change on the nodal planes of the aftershocks and calculating the percentage of events consistent with Coulomb triggering and (2) constructing a 2-D map of Coulomb stress resolved onto 2-D optimally oriented planes and computing the correlation coefficient between the positive and negative areas and the locations of the aftershocks, see section 2.2. The significance of these results is estimated by comparison with several null hypotheses, described in section 2.3.

2.1. Slip Distributions

[13] We here propose a typical, realistic time-indexed suite of slip distributions, as they would become available for a "standard" large earthquake, and apply it to the specific case of the Landers earthquake. Three time indices are distinguished: (1) early models (inverted from worldwide or regional seismic network data) available within hours following the main shock, (2) intermediate models incorporating surface rupture information, available within a few hours to days, and (3) detailed slip inversions, with a time index ranging from hours to weeks depending on the data (teleseismic, strong motion, geodetic) and the inversion procedure. The individual models are described below and more detailed information is given in Table 1.

2.1.1. Early Models

[14] The earliest information on the location and magnitude of the Landers event would have been available from California Institute of Technology/Southern California Earthquake Center and from the National Earthquake Information Center (NEIC). Because the California Institute of Technology solution has subsequently been updated, in the following analysis we choose the NEIC PDE (preliminary determination of epicenters) location.

[15] The initial magnitude reported for the Landers earthquake was M_s = 7.6 and we use the empirical relations of *Wells and Coppersmith* [1994] to calculate both the rupture area and the slip. For a M_s = 7.6 strike-slip earthquake, we find an expected rupture area of 139 × 20 km, a mean slip of 3.31 m, and a maximum slip of 6.28 m. One of the two possible nodal planes has a strike of 355° and a rake of

180°, and as the earthquake occurred in southern California which is dominated by NW-SE trending right-lateral strike-slip faults, this plane is chosen as the fault plane. Immediately following the earthquake, no surface-rupture information would have been available and hence it would have been impossible to know whether the event ruptured unilaterally to either the NW or the SE, or whether the rupture was bilateral. Although we could, of course, test all three assumptions, in practice a decision would have to be made and hence, lacking further information, we assume strict bilateral rupture and place the epicenter at the midpoint of the failed segment. (Note that, rather than the ~$10^{0.9M}$ scaling used here for the mean slip, we could have for example used a ~$10^{0.75M}$ relation consistent with the LW model of *Scholz* [1990] for earthquakes rupturing the whole thickness of the schizosphere. This would imply a relatively larger slip for these simple models).

[16] An additional unknown is the distribution of slip within the event. Although the empirical relations give values for mean and maximum slip, we have no way of knowing the actual distribution. We therefore consider three cases: In the first the distribution of slip is uniform and the entire fault slips 3.31 m (this solution is called "neic" in Figures 3–6); in the remaining two we apply a taper that decays with distance from the maximum slip at the fault center according to $\exp(-(r/L)^n)$ where r is the distance from the center of the fault, L is the length of the faults, and n is a parameter controlling the sharpness of the decay (the larger n, the more abrupt the decay). Here we choose $n = 4$ (neictapf) and $n = 2$ (neictapc) as these values produce near zero slip at the edges with the correct value of the mean slip, fix the maximum slip at the values predicted by *Wells and Coppersmith* [1994] and adjust the number of cells so that the mean slip approximately equals the predicted mean (see Table 1 for details of this and all subsequent slip models).

[17] Within hours of the Landers earthquake, the Harvard quick CMT solution would have been available. This solution has a very different hypocentral location from the NEIC solution as well as a smaller magnitude M_w = 7.3. This magnitude change strongly affects the assumed size of the rupture plane; the empirical relations give an area of 90 × 16 km, a mean slip of 1.78 m, and a maximum slip of 3.08 m. As before, one plane is consistent with California tectonics, and hence we assign the event a strike of 341° and a rake of 172°. Again, we assume bilateral rupture and consider three cases, uniform (hcmt) and tapered with $n = 4$ (hcmttapf) and $n = 2$ (hcmttapc).

2.1.2. Intermediate Models

[18] The Landers earthquake had significant surface rupture [*Sieh et al.*, 1993] and information about surface breaks was available within a few days. We construct a slip model by digitizing the surface rupture depicted in Figure 1 of *Spotila and Sieh* [1995] and assign a uniform slip of 1.78 m to each of the 11 segments (surfrup). While this is clearly unrealistic, we have no a priori method of distinguishing the slip between the different segments and we choose not to use measured surface slip values both because the relation between surface and deep slip is never straightforward and that information would not have been available quickly enough to be of use in the forward modeling.

[19] In order to further test the importance, or otherwise, of including detailed slip information we construct an

Table 1. Slip Models Used in This Study[a]

Slip Model	Number of Segments	Segment	Number of Cells (s)	Number of Cells (d)	Center Latitude	Center Longitude	Strike	Dip	Rake	Length	Width	Maximum Slip	Minimum Slip	Mean Slip
neic	1													
		1	1	1	34.20	−116.44	355	90	180	139	20	3.31	3.31	3.31
neictapf	1													
		1	235	1	34.20	−116.44	355	90	180	139	20	6.28	0.00	3.36
neictapc	1													
		1	225	1	34.20	−116.44	355	90	180	139	20	6.28	0.01	3.36
hcmt	1													
		1	1	1	34.65	−116.65	341	90	172	90	16	1.78	1.78	1.78
hcmttapf	1													
		1	145	1	34.65	−116.65	341	90	172	90	16	3.08	0.00	1.74
hcmttapc	1													
		1	135	1	34.65	−116.65	341	90	172	90	16	3.08	0.02	1.77
surfrup[b]	11													
		1	1	1	34.16	−116.45	344	90	180	5	16	1.78	1.78	1.78
		2	1	1	34.20	−116.46	357	90	180	9	16	1.78	1.78	1.78
		3	1	1	34.28	−116.46	332	90	180	7	16	1.78	1.78	1.78
		4	1	1	34.30	−116.48	8	90	180	5	16	1.78	1.78	1.78
		5	1	1	34.31	−116.45	336	90	180	24	16	1.78	1.78	1.78
		6	1	1	34.43	−116.48	328	90	180	25	16	1.78	1.78	1.78
		7	1	1	34.50	−116.54	0	90	180	1	16	1.78	1.78	1.78
		8	1	1	34.57	−116.59	310	90	180	7	16	1.78	1.78	1.78
		9	1	1	34.61	−116.65	341	90	180	3	16	1.78	1.78	1.78
		10	1	1	34.64	−116.67	330	90	180	3	16	1.78	1.78	1.78
		11	1	1	34.65	−116.67	319	90	180	8	16	1.78	1.78	1.78
simpflts	3													
		1	1	1	34.23	−116.44	355	90	180	30	15	1.78	1.78	1.78
		2	1	1	34.42	−116.48	334	90	180	27	15	1.78	1.78	1.78
		3	1	1	34.57	−116.60	320	90	180	36	15	1.78	1.78	1.78
wald	3													
		1	10	6	34.23	−116.44	355	90	180	30	15	5.89	0.00	1.58
		2	9	6	34.42	−116.48	334	90	180	27	15	6.92	0.00	3.14
		3	12	6	34.57	−116.60	320	90	180	36	15	6.57	0.00	1.54
hernandez	3													
		1	5	3	34.11	−116.43	355	90	180	25	15	6.10	−0.20	1.46
		2	5	3	34.33	−116.45	339	90	180	25	15	6.70	−0.10	3.07
		3	6	3	34.54	−116.55	317	90	180	30	15	5.20	−0.20	1.28
bbcal	1													
		1	1	1	34.20	−116.83	48	90	0	25	10	0.28	0.28	0.28
bbcal	1													
		1	1	1	34.20	−116.83	318	90	180	25	10	0.28	0.28	0.28
bbjones[b]	2													
		1	1	1	34.21	−116.84	320	90	180	15	10	0.28	0.28	0.28
		2	1	1	34.14	−116.88	50	90	0	15	10	0.28	0.28	0.28

[a]For each model, we include the number of segments (each with an independent orientation), the number of cells or subsegments along strike and dip (each having the same orientation as the segment), the coordinates of the segment starting point, the orientation and rake of each segment, the length and width of the segment, and the maximum, minimum, and mean slip. Note that these values are equal under the assumption of uniform slip and that the number of cells in the tapered slip solution is chosen so that the mean slip approximately equals the empirical values.

[b]The coordinates listed are the segments' endpoints.

additional intermediate model based on the simplified fault geometry of *Wald and Heaton* [1994]. This simplified model (simpflts) contains three segments with strikes (from S to N) of 355°, 334°, 320° and lengths of 36, 27, 36 km respectively, each with uniform slip of 1.78 m.

2.1.3. Detailed Slip Inversions

[20] Two detailed slip distributions are available. *Wald and Heaton* [1994] combined local, teleseismic, and geodetic information to invert for slip, whereas *Hernandez et al.* [1999] used SAR, strong motions, and GPS measurements to do the same. Here we consider both, the combined solutions of *Wald and Heaton* [1994] (wald) and *Hernandez et al.* [1999] (hernandez), and compare the results of the approximate solutions to those of the more detailed solutions.

2.1.4. Inclusion of the Big Bear Earthquake

[21] Approximately 3 hours after the Landers earthquake, the $M_w = 6.4$ Big Bear aftershock occurred. Although well away from the Landers rupture, this aftershock could be

expected to perturb the stress field and hence it might be reasonable to re-calculate the Coulomb stress after this event by including its slip distribution in the boundary element computation. The focal mechanism for the event shows either right-lateral strike slip on a NW trending fault or its conjugate, left-lateral slip on a NE trending fault. The latter is consistent with an aftershock on a fault plane conjugate to the Landers rupture.

[22] The California Institute of Technology magnitude of 6.4 implies a rupture area of 25 × 9 km and a mean slip of 0.275 m. No surface rupture was observed, so we assume that the rupture extends between 6 km and 15 km depth. The event was widely believed to have occurred on the conjugate fault plane and hence our first solution is for a NE trending fault, assuming bilateral uniform slip, and the time index is the first day (bbcal). Because there is no surface rupture, and there is still today some controversy as to whether the event was left- or right-lateral, we also
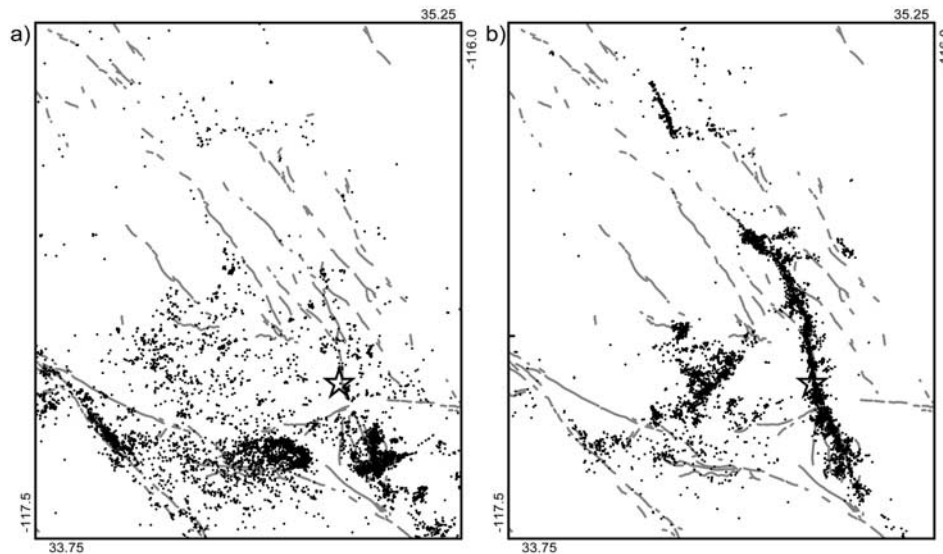
Figure 1. All seismicity from *Hauksson* [2000] catalog occurring within spatial bounds 33.75° to 35.25°N and −117.5° to −116° W and temporal bounds listed below. All depths and all magnitudes are included. Magnitude-frequency distributions show that subsets are complete to approximately $M = 2.3$. Faults shown are historical and Quaternary structures from *California Division of Mines and Geology* [2000] digital fault map. Large star shows Landers epicenter. (a) 5845 events occurring between 1 January 1971 and 27 June 1992. (b) 7282 events occurring between 28 June 1992 and 27 June 1993.

construct an alternative solution assuming bilateral NW trending right-lateral strike-slip, with the same rupture length and slip (bbcalrl). *Jones and Hough* [1995] modeled the event with an empirical Green's function approach and concluded that it ruptured both planes; we therefore construct a third solution based on based on both planes slipping but with a simpler distribution of slip (bbjones). The time index of the last solution is clearly months but the time index of the right-lateral solution is less obvious. In practice, we might envisage that an alternative solution might be attempted if the initial stress field were not in good agreement with the observed aftershocks, in other words that the aftershock activity might be used to update the slip distribution.

2.2. Quantifying Success

[23] We develop two tests for quantifying the capacity of each stress map to correctly predict or explain the aftershock distribution. The first test is based on the agreement between the geometry of the aftershocks and the stress perturbation: are the aftershocks correctly oriented compared to the imposed stress? The second test is a more direct correlation measure between the spatial distributions of the actual and predicted aftershocks. The significance of the tests is assessed by using several null hypotheses.

2.2.1. Seismicity Data

[24] *Hauksson* [2000] relocated more than 305,000 earthquakes that occurred in southern California between 1971 and 1998 using a new 3-D velocity model; the data, including focal mechanisms, is available through the Southern California Earthquake Data Center (www.scecdc.scec.org). From this data, we select, in a rectangular area within the latitude bounds 33.75° to 35.25°N and longitude bounds

−117.5° to −116°W (encompassing virtually all Landers related events), all 7282 events in the year following it (aftershocks) and all 5845 events occurring between 1971 and the time of the Landers earthquake (preshocks); see Figure 1. Many of the latter are aftershocks of the Joshua Tree earthquake that occurred about 2 months prior to Landers, at the southern end of the Landers rupture. Note that if there are two possible focal mechanism for the same event, we treat each as a separate earthquake.

2.2.2. Test 1: Proportion of Focal Mechanisms Consistent With Coulomb Triggering

[25] For each slip distribution, we calculate the tensorial stress perturbation at the location of every aftershock. Because of the ambiguity between fault and auxiliary planes, we resolve the stress tensor into shear (in the appropriate rake direction) and normal components on each plane. The test consists of computing the number of times both, only one, or none of the two nodal planes are consistent with the Coulomb stress, i.e., the stress is positive. This measure can be ambiguous since the correct fault plane is not known a priori. (This issue was examined by *Hardebeck et al.* [1998], who first used this test, *Anderson and Johnson* [1999], and also more directly by *Seeber and Armbruster* [2000], who selected a nodal plane based on correlation and regional tectonics arguments).

2.2.3. Test 2: Spatial Correlation Between Aftershocks and Stress Map

[26] We further test our results by computing stress maps and comparing them to the observed spatial distribution of events. To do so, we need to interpret the (tensorial) stress maps in terms of presence/absence of aftershock triggering (hence a binary field). Keeping in mind that such an interpretation should reflect the practical use of Coulomb

modeling and therefore should not be too computationally involved, we proceed as follows: At every point on a regular 100×100 grid, and for each slip distribution, we compute the strike of the 2-D right-lateral optimally oriented plane; in other words we assume a dip of $90°$ and a rake of $180°$ and a uniaxial regional stress field with $\sigma_1 = 100$ bars, oriented N7°E [*King et al.*, 1994]. We choose 2-D instead of 3-D optimally oriented planes because the majority of the Landers aftershocks occur on near-vertical strike-slip structures [*McCloskey et al.*, 2003] and because the orientation and rake of 3-D optimally oriented planes is extremely sensitive to the vertical component of the regional stress field.

[27] At each point on the grid, we resolve the tensorial stress perturbation into Coulomb stress on a plane with the appropriate orientation and assumed rake. We then associate
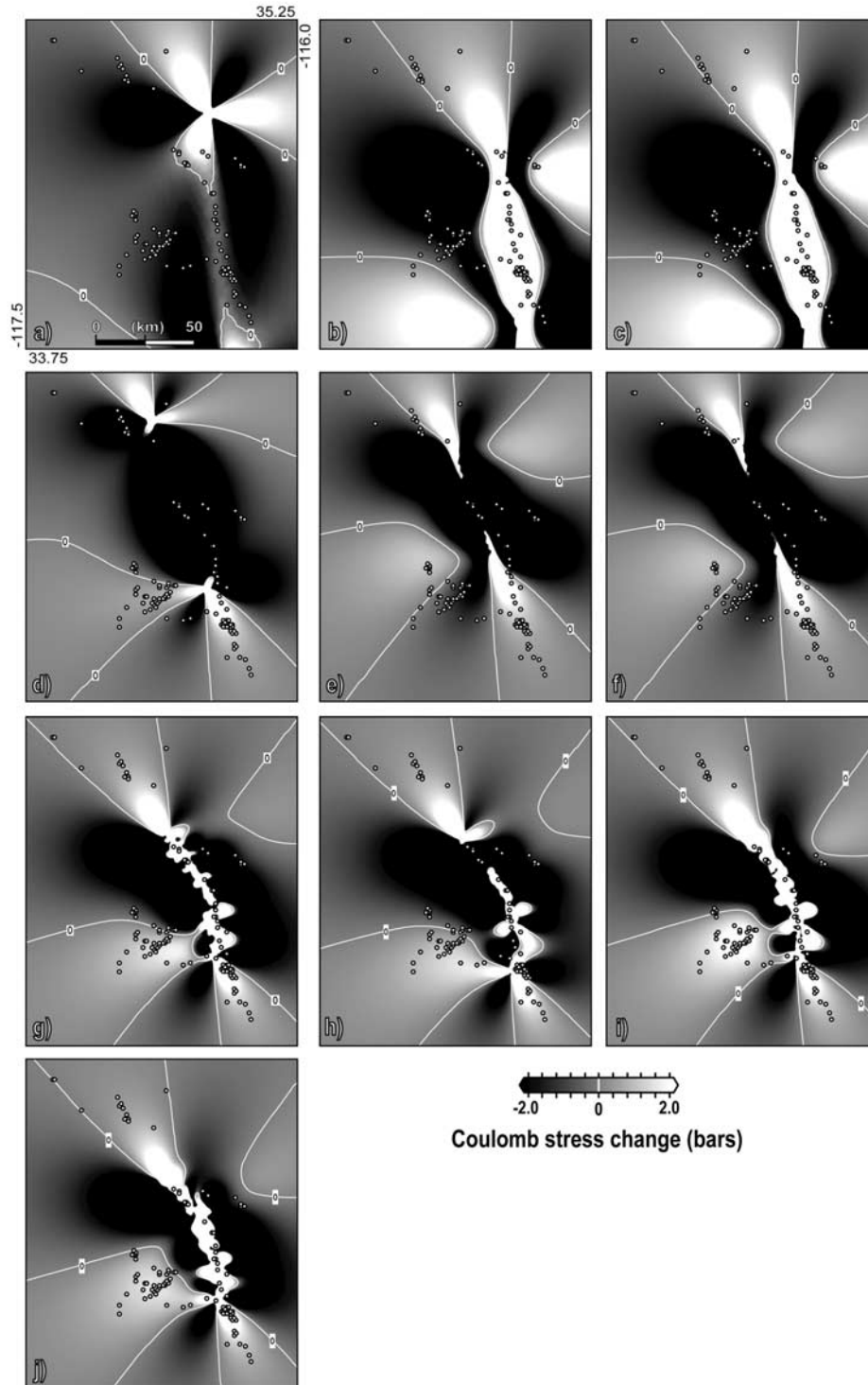
Figure 2.

every event with its nearest grid point and compute the correlation coefficient between the sign of the stress at each grid point and the presence or absence of one or more earthquakes. Note that this technique includes a penalty for area and thus distinguishes between a map that correctly predicts the presence or absence of aftershocks with respect to the stress field and one in which the entire stress field is positive and hence without predictive value.

2.2.4. Significance of the Results

[28] In order to estimate how significant is the success of a given stress map in explaining the aftershocks, we compare these results with those obtained using various null hypotheses. These are different for the two tests. They correspond to very simple, or even crude, prediction models that a seismologist could guess based on very limited information about the main shock. Significantly better test results for the Coulomb stress maps compared to such models will then prove the capacity of these maps in helping to forecast the most likely regions of increased and decreased seismicity.

[29] For the first test, we define three null hypotheses:

[30] 1. The test is performed on the aftershocks, but with random focal mechanisms. These are generated at each aftershock location by randomly choosing a strike between 0° and 360°, dip between 0° and 90°, and rake between 0° and 360°, then computing the appropriate auxiliary plane.

[31] 2. The test is performed on the aftershocks, but their focal mechanisms are shuffled randomly. The focal mechanisms are shuffled by going through the entire aftershock list, randomly picking the number of another event in the list, and swapping the focal mechanisms of the two. This process is repeated 100 times over the entire list to ensure that the resultant focal mechanisms are well randomized.

[32] 3. The test is performed on the preshocks with their actual focal mechanisms.

[33] For the second test, two null hypotheses are considered:

[34] 1. No information is available, so only a purely random distribution can be postulated. These events are created by randomly choosing the same number of points as there are preshocks and populating each of these points with an event.

[35] 2. The off-fault aftershocks are expected to be spatially distributed similarly to preseismicity, as both "illuminate" active structures present in the surroundings of the causative fault. This null hypothesis will therefore measure how appropriate is the Coulomb model in distinguishing between preseismicity and postseismicity.

[36] Similarly to the suite of slip distributions, these null hypotheses clearly correspond to more and more refined knowledge of the main shock and its aftershocks. Notice that, for this second test, only a pixel-by-pixel correlation is performed, so that, for the first null hypotheses, it is insensitive to the clustering of the modeled random distribution (random, self-similar distributions mimicking the fractal characteristics observed in real aftershock sequences would lead to the same statistics for this null hypothesis, as long as the relative proportion of triggered/inhibited pixels stay the same).

[37] Monte Carlo simulations are performed for the first two null hypotheses of test 1 and both of test 2 in order to produce a full distribution of test results that can be compared to the results of the Coulomb models.

3. Results

[38] The stress fields on 2-D optimally oriented planes produced by the different slip models (assuming $\mu = 0.4$) are shown in Figure 2. The top three diagrams show the neic-produced stress maps; note that the southern end of the rupture extends below the bottom axis as the magnitude-based rupture length was 139 km and strict bilateral rupture was assumed. Qualitatively, none of the stress maps are consistent with the pattern of $M > 4$ aftershocks. Note, however, that the tapered solutions give dramatically different results adjacent to the fault zone than the assumption of uniform slip. The second set of diagrams shows the stress maps for the Harvard CMT slip solutions; although the event is mislocated, many aftershocks occur in regions of positive Coulomb stress. Unlike the neic-based stress map above, the tapered slip solutions look similar to that of uniform slip; in other words, positive stress close to the fault is not observed. This appears to be a geometric effect caused by the orientation of the fault plane with respect to the regional stress field and the smoothness of the taper; compare Figures 2d–2f to Figure 2h, which is based on uniform slip. Here the small southern segments with a more N-S orientation have positive stress adjacent to the fault zone while the longer, NW striking segment experiences negative Coulomb stress adjacent to the fault.

[39] Figure 2g shows the stress map based on the surface rupture assuming uniform slip, while Figure 2h shows the map assuming the rupture geometry suggested by *Wald and Heaton* [1994] but with uniform slip. Qualitatively the two are similar although the former has positive stress along the entire fault zone. Figures 2i and 2j show the stress pertur-

---

Figure 2. Maps of Coulomb stress for each Landers slip model, computed on 2-D optimally oriented planes at the intermediate depth of 7.5 km, assuming a uniaxial regional stress field of 100 bars oriented N7°E and that $\mu = 0.4$. Dark colors represent areas of negative Coulomb stress, lighter colors represent positive stress, and white contours represent the zero stress boundary. Scale ranges from -2 to 2 bars for all diagrams. Circles represent the $M > 4.0$ earthquake that occurred in the first year following the Landers event. (a) Stress based on neic solution. Note that the white contours do not enclose the fault zone; although the stress map is light grey along the fault zone, only small portions of the fault experience positive Coulomb stress. (b) Stress for tapered neic solution with $n = 4$ (see section 2.1.1). (c) Tapered neic solution with $n = 2$. (d–f) Stress map for hcmt uniform, tapered $n = 4$ and tapered $n = 2$ slip models. Note negative stress along fault zone for tapered slip models, in contrast to neic models. This is a geometrical effect due to the fault orientation with respect to the regional stress field (see text). (g) Stress field based on mapped surface rupture, assuming uniform slip. (h) Stress assuming fault geometry of *Wald and Heaton* [1994] but assuming uniform slip. (i) Stress map based on slip model of *Wald and Heaton* [1994]. (j) Stress based on slip distribution of *Hernandez et al.* [1999].
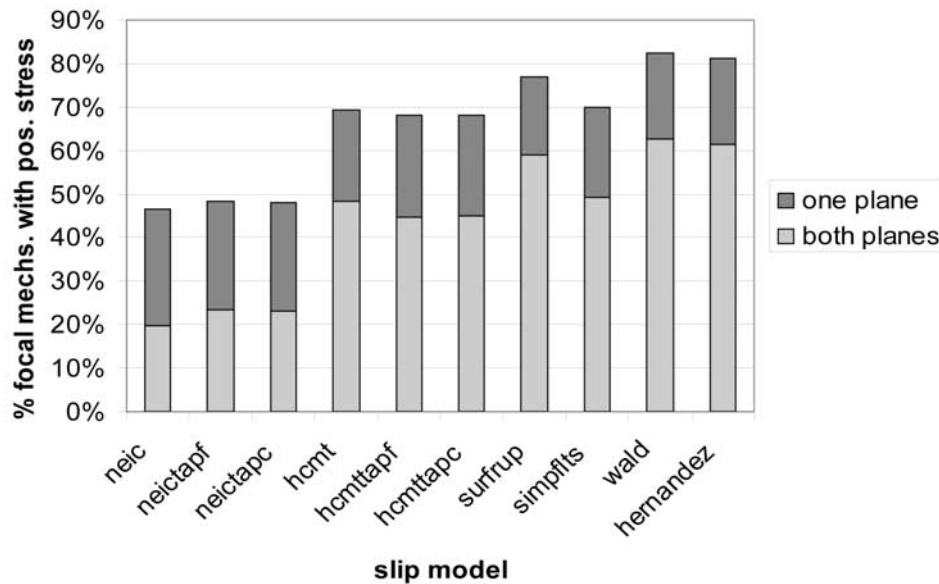
Figure 3. Percentage of aftershock focal mechanisms experiencing positive Coulomb stress on both (light grey) or a single (dark grey) nodal plane for each slip model assuming that the coefficient of friction $\mu = 0.4$. Model names are defined in the text, section 2.1, and in Table 1.

bations calculated from the detailed slip inversions of *Wald and Heaton* [1994] and *Hernandez et al.* [1999], respectively. In appearance the two are very similar and primarily differ from the previous pair immediately adjacent to the fault trace and in the large lobe of positive stress to the SW.

[40] The percentage of the 7282 aftershocks consistent with Coulomb triggering is shown in Figure 3 for each of the 10 Landers slip models. For each model, we plot the percentage of events for which both nodal planes experience a positive Coulomb stress change (resolved in the rake direction) and the percentage for which the change in Coulomb stress is only positive for one plane. The simplest model, based on the neic solution, is clearly the worst, with only 20% of events having both planes consistent with Coulomb triggering and another 25% of events with at least one consistent nodal plane. The tapered variations give almost identical results. The hcmt solution does much better, with 48% of events having 2 consistent nodal planes and 69% at least one consistent plane. In both cases the tapered slip solutions give similar, but slightly worse, results than the assumption of uniform slip. The surface rupture solution is noticeably better, with 59% of events having 2 consistent nodal planes and 77% at least one consistent plane. The *Wald and Heaton* [1994] simplification is similar to the CMT solutions, with 49% and 70% consistency. Perhaps not surprisingly, the detailed slip distributions of *Wald and Heaton* [1994] and *Hernandez et al.* [1999] give the best, and nearly identical, results, 63% and 62%, respectively, of focal mechanisms with both nodal planes experiencing Coulomb stress, and 83% and 81%, respectively, with at least one positive plane.

[41] The comparison of these results with the null hypotheses is shown in Figure 4 where we plot, for each slip model, the percentage of aftershocks, preshocks, and shuffled and random focal mechanisms with

one or more planes experiencing positive Coulomb stress. The correspondence between the stress field and the aftershocks is less than for the null hypotheses for all the neic solutions, slightly greater for hcmt and simpflts, and greater still for surfrup and the detailed slip distributions. Additionally, the randomly shuffled focal mechanisms exhibit a better fit to the stress field than either the purely random mechanisms or the preshocks for these latter three models.

[42] The correlation between the aftershock locations and the stress fields (computed on 2-D optimally oriented planes as described above) is shown in Figure 5. Again, the surfrup, wald, and hernandez solutions do best, but here we see a dramatic difference between the tapered and untapered versions of the neic distribution. This is clearly due to the region of positive Coulomb stress surrounding the fault zones for the tapered solutions; however, note that neither model does better for the aftershocks than for the preshocks. Unlike Figure 4, with this measure we see a large difference between the hcmt stress maps and simpflts, with the latter doing much better than random (but the same within error for the preshocks) while the hcmt models are much worse and no better than either random or the preshocks.

[43] All the results presented to this point have been based on a coefficient of friction of $\mu = 0.4$. Although laboratory experiments generally find that friction varies between about 0.5 and 0.7 [*Jaeger and Cook*, 1979], Coulomb modelers have suggested widely varying values for the "best" coefficient of friction, $\mu = 0.0$ [*Kagan and Jackson*, 1998], $\mu = 0.4$ [*Hardebeck et al.*, 1998], and $\mu = 0.8$ [*Seeber and Armbruster*, 2000]. We therefore investigate the effect of μ by computing stress changes for each model values of $\mu = 0., 0.1, \ldots 0.9$. These results are shown in Figure 6 where we observe that, with the exception of neic uniform slip versus neic tapered slip, the relative
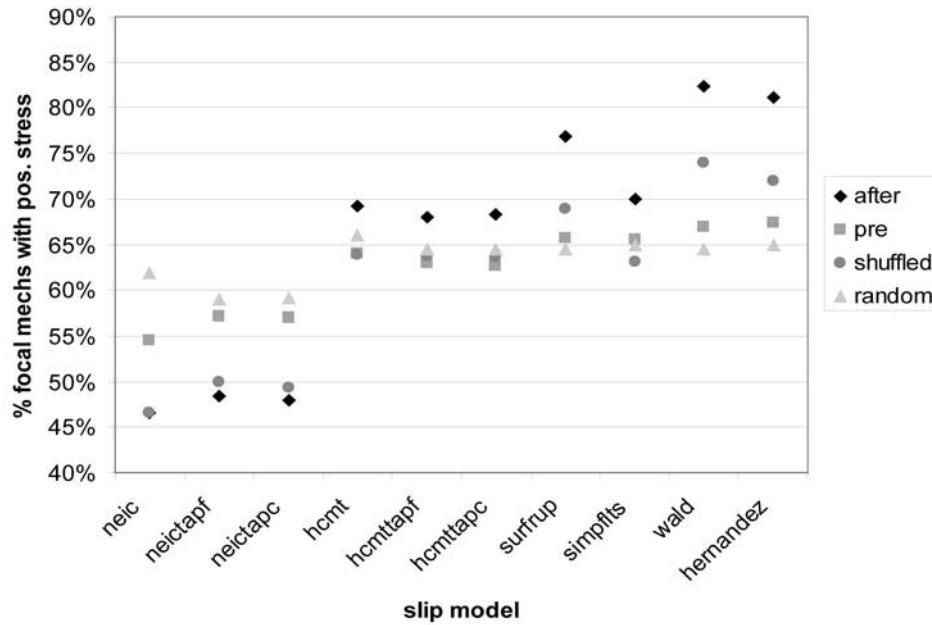
Figure 4. Comparison (for each slip model) of percentage of aftershock focal mechanisms experiencing positive Coulomb stress on one or more nodal planes with same stress field resolved onto nodal planes of preshocks, shuffled focal mechanism, and random focal mechanisms. Again, $\mu = 0.4$. Each "shuffled" and "random" point represents the mean of 10 realizations; error bars are less than 1% and are not shown in this or subsequent figures. Note that the correspondence between the stress field and the aftershocks is greatest for the models based on the surface rupture and the detailed slip distributions, whereas the correspondence between the stress and the aftershocks is worse than the null hypotheses for all of the neic solutions.
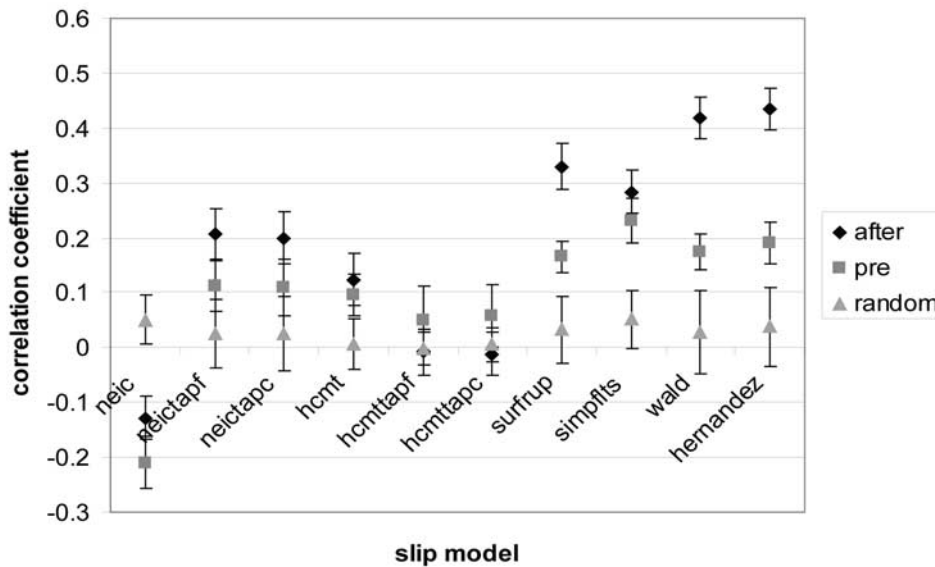
Figure 5. Correspondence between the spatial distribution of earthquakes and the stress fields computed on 2-D optimally oriented planes ($\mu = 0.4$) at a depth of 7.5 km for each slip model. The effect of positive stress along the fault zone for the tapered neic solutions is clearly seen in the positive correlation between stress and aftershocks that is not observed for the uniform slip case. The only other models to do better than random are surfrup, simpflts, wald, and hernandez. However, within error, simpflts corresponds equally well with the preshocks, as do the tapered neic models.
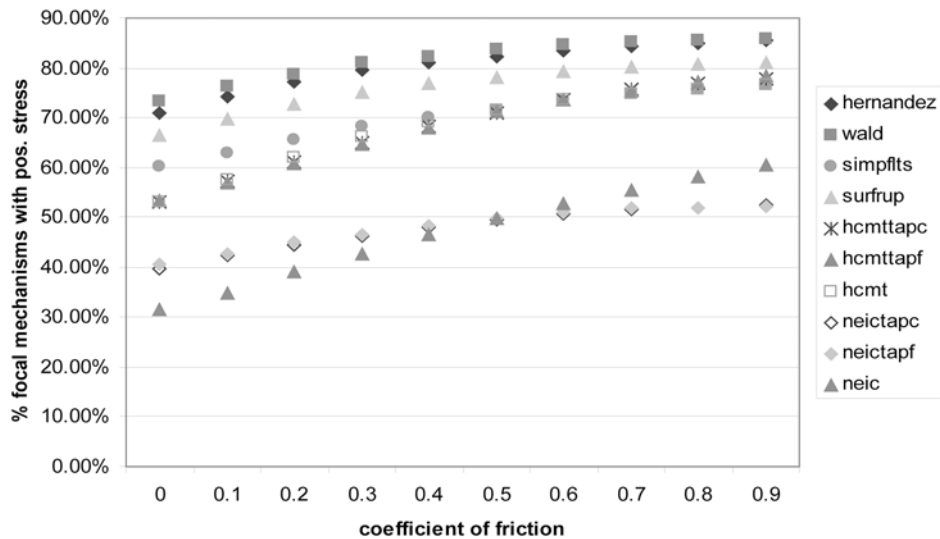
Figure 6. Effect of the coefficient of friction on the percentage of focal mechanisms with one or more planes experiencing Coulomb stress. With the exception of neic uniform outperforming neic tapered at higher μ, relative predictive capacity of the models remains unchanged. Apparent increase in percentage of consistent planes is an artifact of the measurement technique; see Figure 7 and the text.

predictive capacity of each model remains the same; that is, wald is better than Hernandez, which is better than surfrup regardless of μ. We also observe that all models have a greater percentage of focal mechanisms experiencing positive Coulomb as μ increases.

[44] Counting the number of aftershocks with positive Coulomb stress on at least one nodal plane is, however, an ambiguous measure with respect to the influence of μ. A simple calculation shows that, in the case of a totally random stress field, on average 50% of the aftershocks are expected to satisfy this test when $\mu = 0$, and this increases to 66.7% at $\mu \gg 1$. This growth comes from the fact that the Coulomb stresses on the two nodal planes tend to become less and less correlated as μ increases, hence increasing the chance that at least one of them has a positive stress. Inversely, the percentage of aftershocks with both nodal planes receiving positive stress decreases with μ (from 50% at $\mu = 0$ to 25% at $\mu \gg 1$) in the random stress field case.

[45] This growth is well observed in Figure 7, where the percentage of aftershocks with at least one nodal plane undergoing a positive stress change is plotted against μ for the wald model and its null hypotheses. The random focal mechanisms are seen to increase from the expected 50% at $\mu = 0$ to a value significantly larger than 66.7% at $\mu \gg 1$, the latter effect being due to the fact that the stress field is
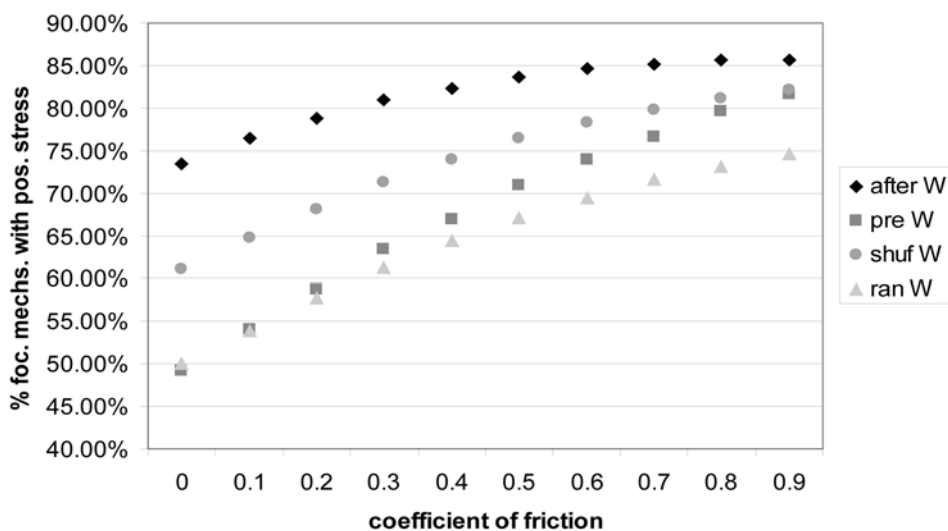

Figure 7. Effect of coefficient of friction on percentage of aftershocks and null hypotheses consistent with Coulomb triggering for wald model. Note that the growth of μ is a purely statistical effect due to the choice of the measure, as shown by the growth of the random case.
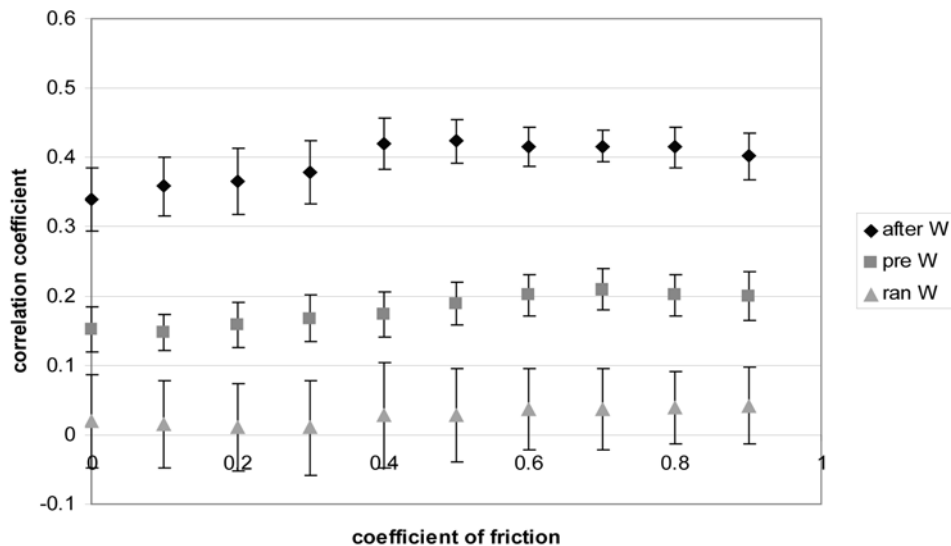
Figure 8. Effect of coefficient of friction on correlation coefficient for wald model. In this measurement technique, nodal plane ambiguity is removed, and little change in the correlation coefficient with μ is observed.

not random and leads more frequently to unclamping than clamping at the locations of the aftershocks (for random aftershock fault geometries this observation goes against the one by *Kagan and Jackson* [1998]). At all values of μ between 0 and 1, the model is seen to significantly better predict the aftershocks than the preshocks, the aftershocks with randomly reshuffled fault geometries, and the aftershocks with random fault geometries.

[46] An important question in this analysis is which value of μ best explains the aftershock distribution for a given stress field. The fact that there exists an automatic increase of the percentage of at least one nodal plane consistent with the Coulomb stress renders the use of this test somewhat difficult for resolving this issue. As a general tendency, the growth with μ is less steep for the actual aftershocks than it is for the various null hypotheses, hence the model could be considered to perform best at μ = 0. However, this measure is certainly not well designed for reliably addressing this question.

[47] The correlation coefficient test does not suffer from the nodal plane ambiguity, and the results are only slightly dependent on the value of μ, as shown in Figure 8 (still for the Wald model). No significant difference between the tested values of μ can be discriminated. Direct inspection of the stress maps with varying μ shows that their general features (position of the lobes) show little sensitivity to the values of the friction coefficient (between 0 and 1), so that the correlation with the seismicity field remains roughly unchanged. (This is true for both 2-D and 3-D optimally oriented planes).

[48] The results presented above include all events irrespective of their proximity to the causative fault. This may affect our results as most aftershocks occur on the fault plane where the stress pattern is strongly affected by the small-scale distribution of slip, details that are unlikely to be captured in even the most sophisticated slip inversions. *Hardebeck et al.* [1998], for example, found a lower percentage of events consistent with Coulomb triggering for

events <5 km from the fault zone than for those between 5 and 75 km distant. Here we examine this effect by systematically excluding events within 1, 2, 5, and 10 km of the fault zone (specific for each slip model) and performing our statistical tests on the remainder. We find that the general picture remains unchanged; the neic and hcmt models perform very poorly, but we do see changes in the four most detailed models. This is shown in Figure 9 where we plot the percentage of focal mechanisms with one or more planes experiencing positive Coulomb stress. A slight increase with exclusion distance is observed for all four models, somewhat greater than that observed in the random case (using the wald and simpflts stress fields) that are shown for comparison. The effect of exclusion distance on the correlation coefficient is shown in Figure 10. Here we observe two distinct groups; when events close to the fault are included, the models surfrup and simpflts perform worse than the detailed slip models, but this difference disappears when only events greater than 5 km from the fault are analyzed.

[49] The Big Bear aftershock (M_w = 6.4) occurred less than 4 hours after Landers, and it is logical to assume that we should include the stress perturbation from it in our calculations. This is complicated, however, by the lack of surface rupture as well as the lack of attention it received, as a consequence the slip distribution is poorly understood. We therefore consider the three slip distributions discussed in section 2.1.4 and combine each with either the Wald or Hernandez detailed solution. These stress patterns are shown in Figure 11 where it is clear that the number of $M > 4$ events in positive stress lobes is less than for the Wald or Hernandez solutions alone (compare to Figure 2). This is shown quantitatively in Figure 12, where the percentage of aftershocks consistent with Coulomb triggering is seen to decrease with the inclusion of Big Bear. Similarly, as shown in Figure 13, in all cases adding the Big Bear stress perturbation decreases the correlation coefficient between the stress fields and the aftershocks. (Note that there are only nine events in our catalog
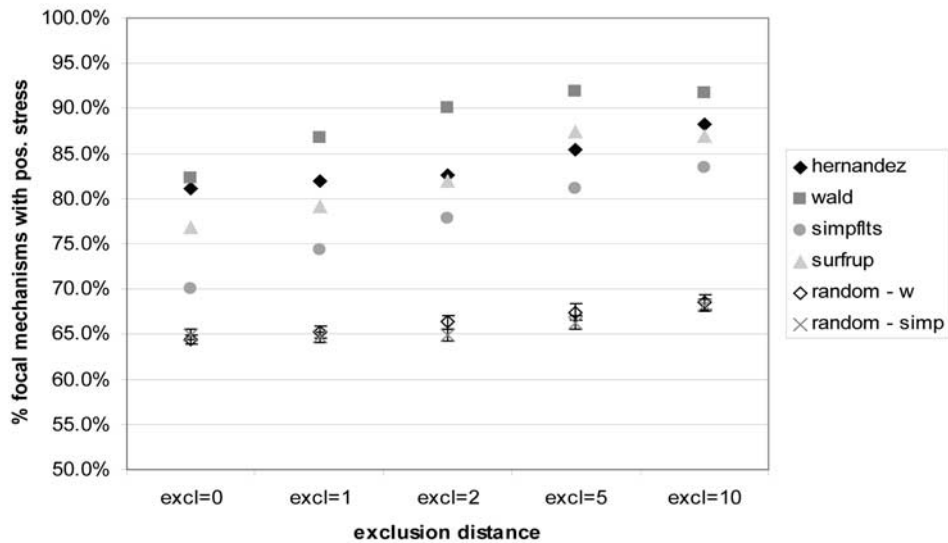
Figure 9. Effect of excluding near-fault events on percentage of aftershock focal mechanisms experiencing positive Coulomb stress for the four most realistic models. For reference, two random cases, based on the simpflts and wald models, are also shown. Note that the number of events considered in the analysis decreases with increasing exclusion distance and depends on the rupture geometry of the particular model. For exclusion (excl) = 0, number of events (nevents) = 7282 for all models; for excl = 1, nevents = 6992 (hernandez), 5875 (wald and simpflts), and 6433 (surfrup); for excl = 2, nevents = 6533 (hernandez), 5154 (wald and simpflts), and 5747 (surfrup); for excl = 5, nevents = 5061 (hernandez), 4477 (wald and simpflts), and 4484 (surfrup); and for excl = 10, nevents = 3930 (hernandez), 3980 (wald and simpflts), and 3900 (surfrup).

between the time of Landers and that of Big Bear, too few to affect the results.)

4. Discussion

[50] As previous authors [*Kilb et al.*, 1997; *Hardebeck et al.*, 1998; *Anderson and Johnson*, 1999; *Seeber and Armbruster*, 2000] have noted, assessing success by computing the percentage of aftershocks experiencing positive Coulomb stress has inherent limitations due to the ambiguity of the nodal plane. One effect of this is shown in Figure 7 where the ambiguity leads to an apparent increase in the percentage of events experiencing positive Coulomb stress as μ increases, but the similar increase in the measure for the
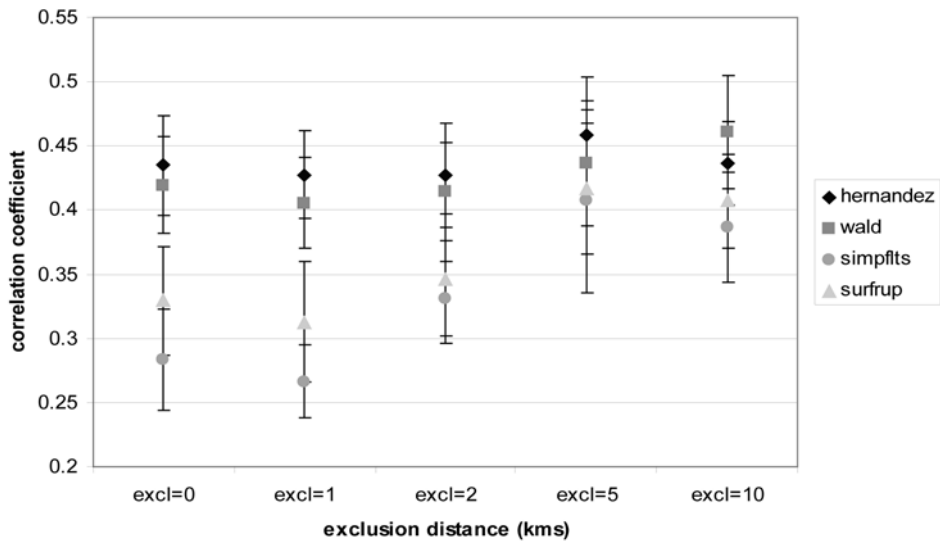

Figure 10. Effect of excluding near-fault events on correlation coefficient. Very close to the fault, the more detailed slip distributions perform better than the simple solutions; at a distance of 5 km the models are equal within error. Note that this is not due to larger error bars with fewer events, as the mean value of the correlation coefficient for the simpler models increases with exclusion distance. The number of events at each distance is given in caption of Figure 9.
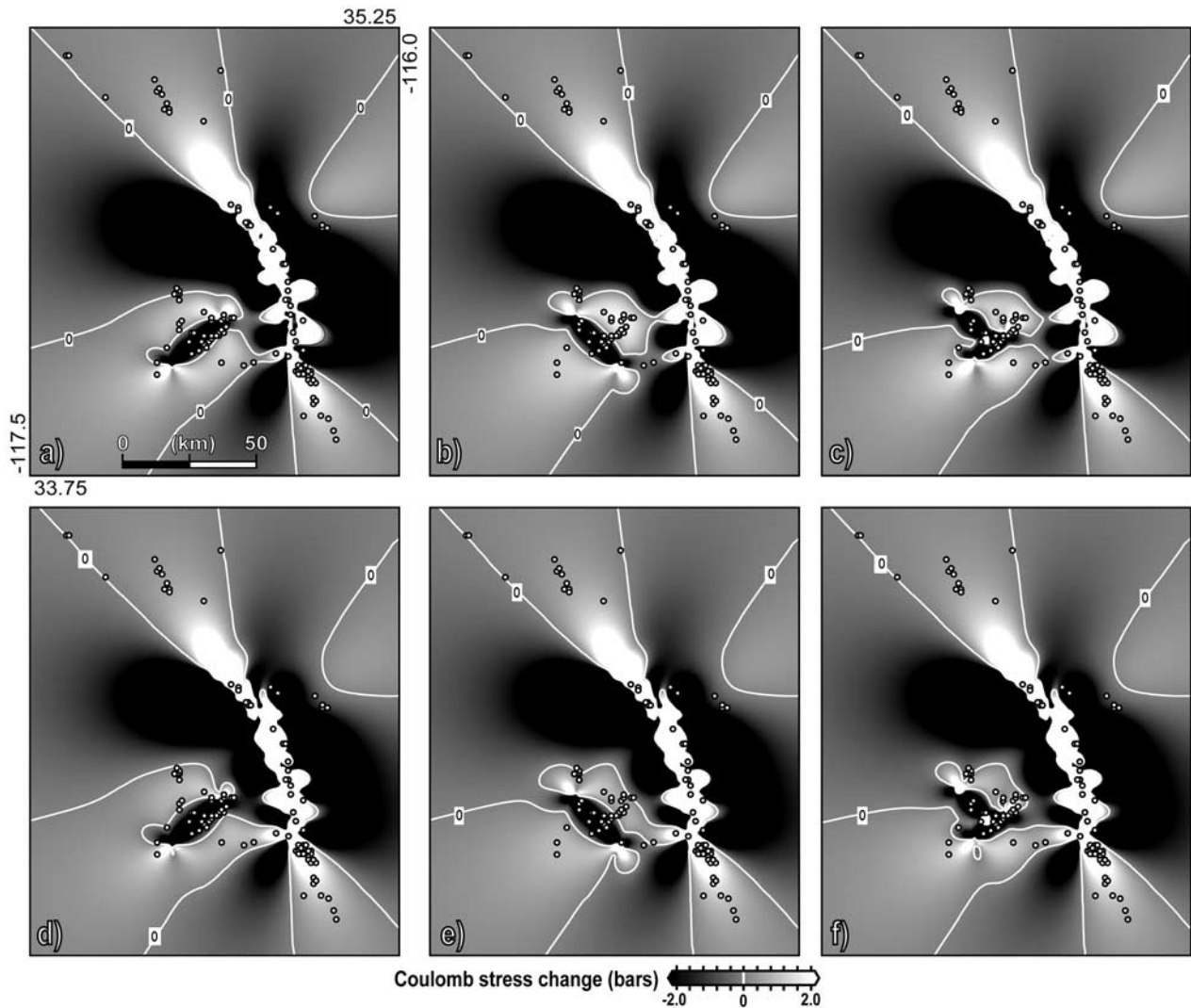
Figure 11. Stress fields computed for Big Bear slip models in conjunction with the (a–c) wald and (d–f) hernandez slip distributions.

random focal mechanisms demonstrates that this is, in fact, an artifact of the analysis technique.

[51] Another problem with this measure is highlighted in Figure 4 where we see that the hcmt slip solutions perform better than the null hypotheses, despite the hypocenter being mislocated. Qualitatively, the hcmt based stress maps show poorer agreement with (at least) the $M > 4$ aftershocks than simpflts (see Figure 2), yet quantitatively the two solutions perform equally well. The reason for this appears to lie in the relation between the regional stress, fault structure, and structures upon which the earthquakes occur. Following *McCloskey et al.* [2003], this relation is illustrated in Figure 14a where the upper portion of the diagram shows the number of 1 km long fault segments binned at 5° intervals between −90° and 90°, and the lower portion of the diagram shows the number of preshock nodal planes binned at 5° intervals between 90° and 270° (where the nodal plane most consistent with the regional trend is chosen). As illustrated by the arrows representing the vector means of each data set, the mean orientations of the fault data and the preshock focal

mechanisms are virtually identical, 328° and 331°, respectively. A very similar relation for the aftershocks is shown in Figure 14b, although there is a slight rotation of the aftershocks to a mean orientation of 326°.

[52] Our interpretation is that all events occur on faults with a limited range of orientations, constrained by the regional structure [*McCloskey et al.*, 2003], and hence only a limited range of aftershock focal mechanisms are possible. If the predicted Coulomb stress field is compatible with triggering events on these structures, then a measure based on comparing the stress field with the aftershock focal mechanisms may give apparently good results, even if there is no causal relation between the two. This interpretation is supported by the observation that randomly shuffled focal mechanisms (Figure 4) show a better fit to the Coulomb stress field than random geometries for the models surfrup, wald, and hernandez owing to, we believe, to the consistency of the stress field from these slip models with the aftershock focal mechanisms, regardless of their location. (The better correspondence of these stress maps with the shuffled aftershocks than with the preshocks may be due to
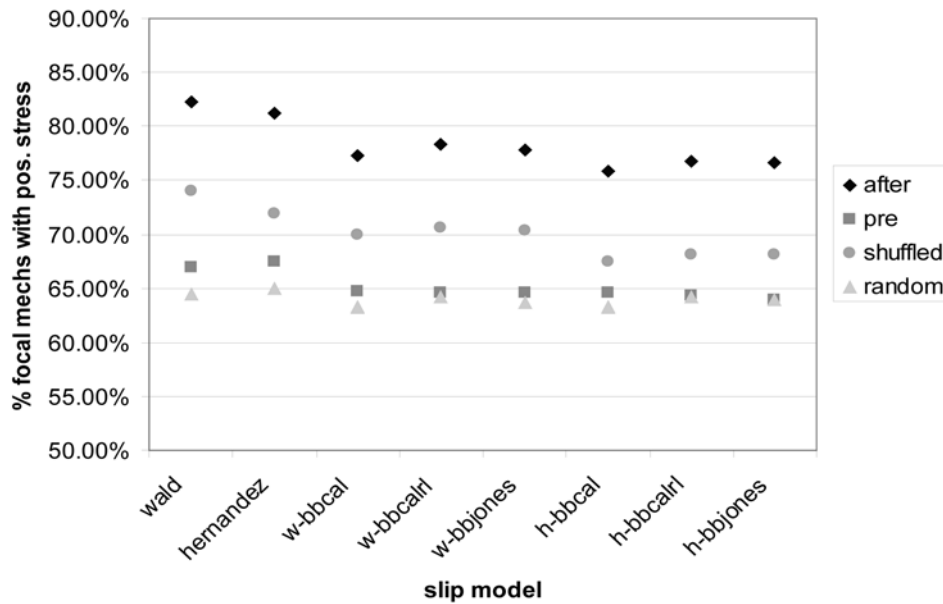
Figure 12. Comparison (for each slip model) of percentage of aftershock focal mechanisms experiencing positive Coulomb stress on one or more nodal planes with same stress field resolved onto nodal planes of preshocks, shuffled focal mechanism, and random focal mechanisms. Again, $\mu = 0.4$ and "shuffled" and "random" points represent the mean of 10 realizations; error bars are less than 1%. None of the models that include Big Bear do as well as those based on the main shock alone.

the slight rotation between the preferred orientations of the two groups of seismic data.)

[53] On the basis of these observations, we believe that a better measure of Coulomb stress is whether the subset of these appropriately oriented faults that experience positive Coulomb stress are activated by the stress change, while those experiencing negative stress are temporarily shut down; in other words, whether a spatial correspondence between stress change and aftershock location is observed. Such a measure must be used with caution, however, as we observe that some very poor models, such as the tapered neic slip solutions, produce better results than randomly placed events. While this clearly results from the positive stress along the rupture plane, we believe that the validity of this measure is best tested against the preshocks; if the stress map shows a better correspondence with the aftershocks than the preshocks, it can be considered a success.
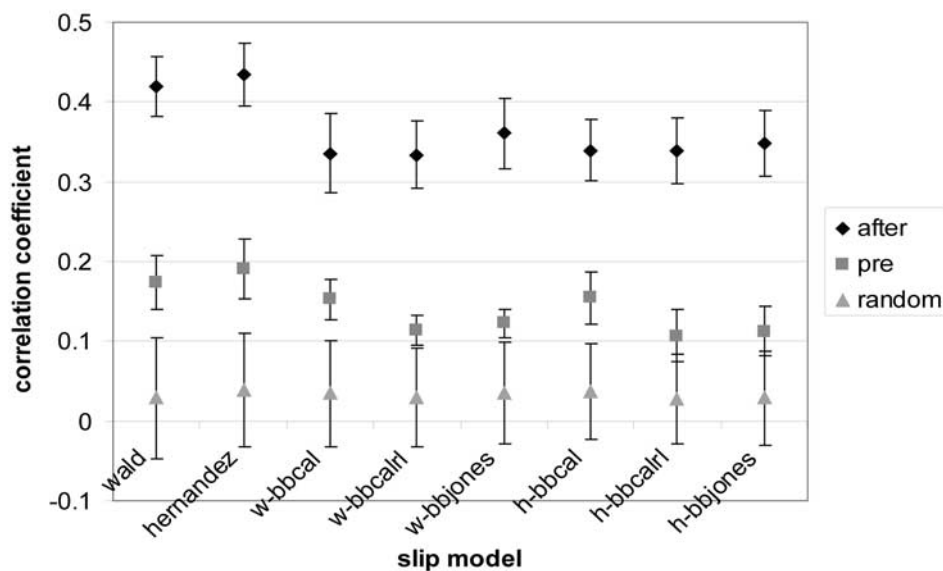

Figure 13. Correspondence between the spatial distribution of earthquakes and the stress fields computed on 2-D optimally oriented planes ($\mu = 0.4$) at a depth of 7.5 km for each slip model. As Figure 12, none of the models that include Big Bear do as well as those based on the main shock alone.
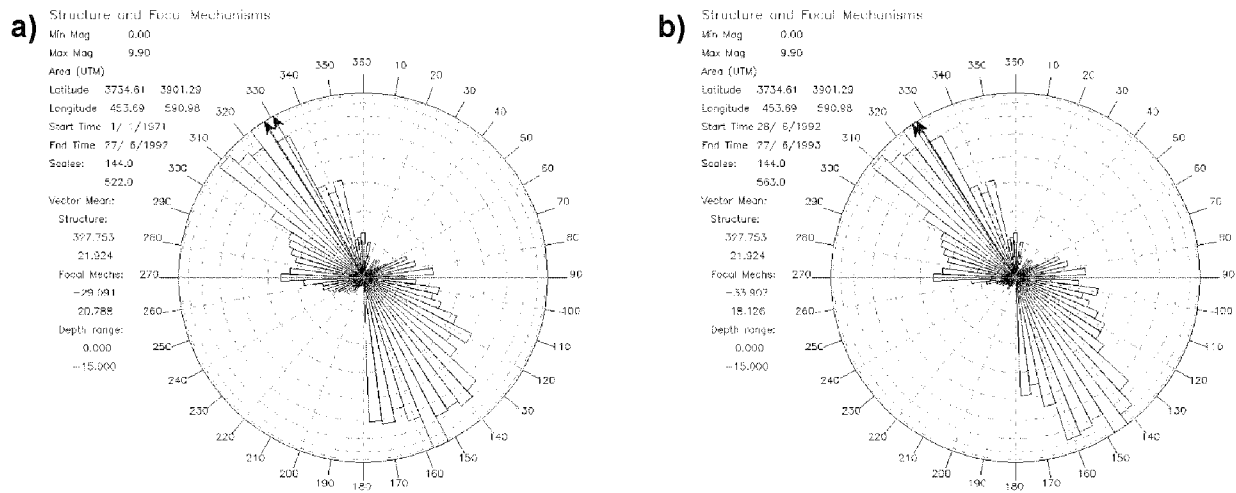
Figure 14. Relation between fault structure and seismic data. In each diagram, the upper quadrant shows the number 1 km long fault segments binned at 5° intervals between −90° and 90°, and the lower portion of the diagram shows the number of earthquake nodal planes binned at 5° intervals between 90° and 270° (where the nodal plane of each focal mechanism most consistent with the regional trend is chosen). Earthquake data are the same as plotted in Figure 1. Arrows represent vector means of both data sets. (a) Preshocks with vector mean of structure of 327.8°, whereas vector mean of preshocks is 330.9°. (b) Aftershocks with vector mean of structure of 327.8°, whereas vector mean of preshocks is 326°.

[54] This test depends, in turn, on the spatial distribution of preshocks as a sufficient number of them must occur in the future stress shadows. We argue that this condition is satisfied in Landers as three of the four most realistic models are better correlated with the aftershocks than the preshocks (Figure 5) when all events are included, while all four are better correlated when events within 2 km of the fault are excluded. (This is because the correspondence between the stress maps and the aftershocks generally increases with exclusion distance for the correct geometry, uniform slip models (Figure 10), while the correspondence with the preshocks does not improve.)

[55] Using this spatial measure, we observe that the correspondence between the stress map (for any given slip model) and the distribution of aftershocks is insensitive to the coefficient of friction assumed in the modeling. This is an important result as it suggests that forward models of Coulomb stress, and hence of likely aftershock locations, will not depend strongly on whichever poorly constrained friction coefficient is chosen by the modeler. Visual inspection of Coulomb stress maps, resolved onto both 2-D and 3-D optimally oriented planes, support this result as the main lobes of positive and negative stress change little with changing μ.

5. Conclusions

[56] Our most important result is that following the Landers earthquake a map of the stress perturbation and hence the areas in which aftershocks were likely could have been constructed within hours to days of the event, as soon as the rupture geometry was well constrained. Although this solution would not have modeled the slip distribution in any great detail, the stress map would have only differed significantly from that based on a time-consuming slip inversion very close to the fault plane. This difference would not have been important from a hazard perspective as any map of potential aftershock hazard would necessarily have included the main shock fault plane.

[57] By contrast, a stress map computed from either the main shock focal mechanism or the Harvard CMT solution would have been poorly correlated with the aftershock distribution. The initial magnitude of the earthquake as reported by NEIC was 0.3 units too large, corresponding to almost 50 km in length, and both the single fault orientation and the assumption of strict bilateral rupture would have led to a very poor representation of the stress perturbation. The CMT solution was a reasonable average of the Landers slip but the mislocation of the moment centroid would have again led to an inaccurate stress map. Assuming tapered instead of uniform slip would not have improved the results significantly.

[58] Inclusion of the largest aftershock, Big Bear, in the stress calculation would have decreased the correlation between the computed stress field and the observed aftershock distribution. Whether this is due to poor understanding of the Big Bear rupture geometry is not clear.

References

Anderson, G., and H. Johnson (1999), A new statistical test for static stress triggering: Application to the 1987 Superstition Hills earthquake sequence, *J. Geophys. Res.*, *104*, 20,153–20,168.

California Division of Mines and Geology (2000), Digital database of faults from the fault activity map of California and adjacent areas, *Map CD 2000-006*, Sacramento, Calif.

Chinnery, M. A. (1963), The stress changes that accompany strike-slip faulting, *Bull. Seismol. Soc. Am.*, *53*, 921–932.

Das, S., and C. H. Scholz (1981), Off-fault aftershock clusters caused by shear-stress increase?, *Bull. Seismol. Soc. Am.*, *71*, 1669–1675.

Hardebeck, J. L., J. J. Nazareth, and E. Hauksson (1998), The static stress change triggering model: Constraints from two southern California aftershock sequences, *J. Geophys. Res.*, *103*, 24,427–24,452.

Harris, R. A. (1998), Stress triggers, stress shadows, and implications for seismic hazard, *J. Geophys. Res.*, *103*, 24,347–24,358.

Harris, R. A., and R. W. Simpson (1992), Changes in static stress on the southern California faults after the 1992 Landers earthquake, *Nature*, *360*, 251–254.

Harris, R. A., R. W. Simpson, and P. A. Reasenberg (1995), Influence of static stress changes on earthquake locations in southern California, *Nature*, *375*, 221–224.

Hauksson, E. (2000), Crustal structure and seismicity distribution adjacent to the Pacific and North American plate boundary in southern California, *J. Geophys. Res.*, *105*, 13,875–13,903.

Hernandez, B., F. Cotton, and M. Campillo (1999), Contribution of radar interferometry to a two-step inversion of the kinematic process of the 1992 Landers earthquake, *J. Geophys. Res.*, *104*, 13,083–13,099.

Hubert-Ferrari, A., A. Barka, E. Jacques, S. S. Nalbant, B. Meyer, R. Armijo, P. Tapponnier, and G. C. P. King (2000), Seismic hazard in the Marmara Sea region following the 17 August 1999 Izmit earthquake, *Nature*, *404*, 269–273.

Jaeger, J. C., and N. G. W. Cook (1979), *Fundamentals of Rock Mechanics*, Chapman and Hall, New York.

Jones, L. E., and S. E. Hough (1995), Analysis of broadband records from the 28 June 1992 Big Bear earthquake: Evidence of a multiple-event source, *Bull. Seismol. Soc. Am.*, *85*, 688–704.

Kagan, Y. Y., and D. D. Jackson (1998), Spatial aftershock distribution: Effect of normal stress, *J. Geophys. Res.*, *103*, 24,453–24,467.

Kilb, D., M. Ellis, J. Gomberg, and S. Davis (1997), On the origin of diverse aftershock mechanisms following the 1989 Loma Prieta earthquake, *Geophys. J. Int.*, *128*, 557–570.

King, G. C. P., and M. Cocco (2001), Fault interaction by elastic stress changes: New clues from earthquake sequences, *Adv. Geophys.*, *44*, 1–38.

King, G. C. P., R. S. Stein, and J. Lin (1994), Static stress changes and the triggering of earthquakes, *Bull. Seismol. Soc. Am.*, *84*, 935–953.

Marsan, D. (2003), Triggering of seismicity at short timescales following Californian earthquakes, *J. Geophys. Res.*, *108*(B5), 2266, doi:10.1029/2002JB001946.

McCloskey, J., S. S. Nalbant, S. Steacy, C. Nostro, O. Scotti, and D. Baumont (2003), Structural constraints on the spatial distribution of aftershocks, *Geophys. Res. Lett.*, *30*(12), 1610, doi:10.1029/2003GL017225.

Nalbant, S., A. Hubert, and G. C. P. King (1998), Stress coupling between earthquakes in northwest Turkey and the north Aegean Sea, *J. Geophys. Res.*, *103*, 24,469–24,486.

Parsons, T., S. Toda, R. S. Stein, A. Barka, and J. H. Dieterich (2000), Heightened odds of large earthquakes near Istanbul: An interaction based probability calculation, *Science*, *288*, 661–665.

Reasenberg, P. A., and R. W. Simpson (1992), Response of regional seismicity to the static stress change produced by the Loma Prieta earthquake, *Science*, *255*, 1687–1690.

Scholz, C. H. (1990), *The Mechanics of Earthquakes and Faulting*, Cambridge Univ. Press, New York.

Seeber, L., and J. G. Armbruster (2000), Earthquakes as beacons of stress change, *Nature*, *407*, 69–72.

Sieh, K., et al. (1993), Near-field investigations of the Landers earthquake sequence, April to July, 1992, *Science*, *260*, 171–176.

Spotila, J. A., and K. Sieh (1995), Geologic investigations of a "slip gap" in the surficial ruptures of the 1992 Landers earthquake, southern California, *J. Geophys. Res.*, *100*, 543–559.

Stein, R. S. (1999), The role of stress transfer in earthquake occurrence, *Nature*, *402*, 605–609.

Stein, R. S., and M. Lisowski (1983), The 1979 Homestead Valley earthquake sequence, California: Control of aftershocks and postseismic deformation, *J. Geophys. Res.*, *88*, 6477–6490.

Stein, R. S., G. C. P. King, and J. Lin (1992), Change in failure stress on the southern San Andreas fault system caused by the 1992 magnitude = 7.4 Landers earthquake, *Science*, *258*, 1328–1332.

Stein, R. S., A. A. Barka, and J. H. Dieterich (1997), Progressive failure on the North Anatolian fault since 1939 by earthquake stress triggering, *Geophys. J. Int.*, *128*, 594–604.

Wald, D. J., and T. H. Heaton (1994), Spatial and temporal distribution of slip for the 1992 Landers, California, earthquake, *Bull. Seismol. Soc. Am.*, *84*, 668–691.

Wells, D. L., and K. J. Coppersmith (1994), New empirical relationships among magnitude, rupture length, rupture width, rupture area, and surface displacement, *Bull. Seismol. Soc. Am.*, *84*, 974–1002.

————————————

D. Marsan, Laboratoire de Géophysique Interne et de Tectonophysique, Université de Savoie, 73376 Le Bourget du Lac cedex, France.

J. McCloskey, S. S. Nalbant, and S. Steacy, Geophysics Research Group, University of Ulster, Coleraine, Co. Derry, N. Ireland, BT52 1SA. (s.steacy@ulst.ac.uk)